ACS Photonics

pubs.acs.org/journal/apchd5

Article

Integrated Molecular Optomechanics with Hybrid Dielectric–Metallic Resonators

Ilan Shlesinger,[§] Kévin G. Cognée,[§] Ewold Verhagen, and A. Femius Koenderink*

Cite This: *ACS Photonics* 2021, 8, 3506–3516

Read Online

ACCESS | Metrics & More | Article Recommendations | Supporting Information

ABSTRACT: Molecular optomechanics describes surface-enhanced Raman scattering using the formalism of cavity optomechanics as a parametric coupling of the molecule's vibrational modes to the plasmonic resonance. Most of the predicted applications require intense electric field hotspots but spectrally narrow resonances, out of reach of standard plasmonic resonances. The Fano lineshapes resulting from the hybridization of dielectric–plasmonic resonators with a broad-band plasmon and narrow-band cavity mode allow reaching strong Raman enhancement with high-Q resonances, paving the way for sideband resolved molecular optomechanics. We extend the molecular optomechanics formalism to describe hybrid dielectric–plasmonic resonators with multiple optical resonances and with both free-space and waveguide addressing. We demonstrate how the Raman enhancement depends on the complex response functions of the hybrid system, and we retrieve the expression of Raman enhancement as a product of pump enhancement and the local density of states. The model allows prediction of the Raman emission ratio into different output ports and enables demonstrating a fully integrated high-Q Raman resonator exploiting multiple cavity modes coupled to the same waveguide.

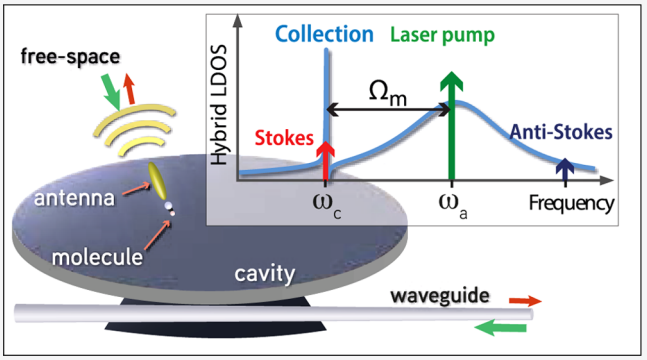

KEYWORDS: *SERS, nanophotonics, plasmonics, optomechanics, integrated photonics*

INTRODUCTION

It is well understood that the electromagnetic enhancement in surface-enhanced Raman spectroscopy (SERS)[1−3] benefits both from the electromagnetic field enhancement of the pump field driving the Raman process and from the plasmonically generated local density of optical states (LDOS) enhancement for the emission at the Stokes and anti-Stokes sidebands.[4−8] It stems from a second-order perturbation description of the two-step Raman process.[6,9] The enhancement will thus depend on the exact response function of the plasmonic system at those frequencies and can be computed using the Green tensor and numerical solvers for nontrivial geometries.[6,10,11] Recently, the new formalism of molecular optomechanics was introduced, showing the analogy of SERS with cavity optomechanics.[12] It describes the Raman process as an optomechanical interaction between a localized plasmonic resonance and a molecule's nuclear motion. The coupling of light and motion stems from a dispersive shift of the plasmonic resonance upon the molecule's vibrational displacement.[10,12−14] The cavity optomechanics viewpoint allows a consistent description of optical forces on the molecule's vibration inducing quantum and dynamical back-action,[14] which were previously described phenomenologically as vibrational pumping and as plasmonic asymmetry factor.[15] Furthermore, with the correct description of coherence in the optomechanical interaction, new phenomena such as collective effects have been predicted,[16] and within state of the art in plasmonic nano- and picocavities,[17] one could envision promising applications such as coherent quantum state transfer[18] and entanglement between photons and phonons[19−21] at high frequencies (1−100 THz), where no cooling is required. Very recent experimental works have already demonstrated mid-IR-to-visible transduction using this scheme.[22,23]

Cavity optomechanics often operates in the so-called "resolved sideband regime", wherein the mechanical frequency exceeds the optical linewidth.[24] This, for instance, is deemed crucial for cooling of macroscopic motion through selectively enhancing anti-Stokes scattering[25] and to reach coherent conversion from photons to phonons and back.[19−21] The molecular optomechanics equivalence would be to have access to optical resonators with linewidths narrower than the vibrational frequency of the molecular species at hand, yet

Received: June 1, 2021
Published: November 16, 2021

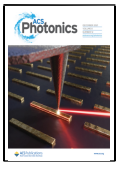

nonetheless exceptionally good confinement of the electric field for large coupling to the Raman dipole. This regime is not easily reached with plasmonics, as resonators typically have quality factors $Q \sim 20$, meaning linewidths larger than or comparable to vibrational frequencies (500−1500 cm^{-1}). Conversely, conventional higher-Q dielectric resonators typically have poor mode confinement and hence poor SERS enhancement.[26] This can in principle be compensated by increasing the quality factor of the cavities to reach SERS enhancements above 10^4 with, for example, whispering gallery modes (WGMs) of $Q \simeq 10^6$.[27] Nonetheless, these narrow optical resonances have linewidths below 1 GHz, 2 orders of magnitudes smaller than usual Raman linewidths, and thus only enhance a small fraction of the vibrational resonance. In the last few years, hybrid photonic−plasmonic resonators have emerged, in which hybrid resonances of dielectric microcavities coupled to plasmonic antennas are used.[28−34] Theoretical and experimental evidence points at plasmonic confinement ($<\lambda^3/10^5$) with microcavity quality factors ($Q > 10^3$).[35,36]

In this work, we report on a semiclassical molecular optomechanics model for waveguide (WG)-addressable multiresonant hybrid photonic−plasmonic resonators coupled to molecular mechanical oscillators. This work has several important novelties. First, in evaluating the SERS enhancement, previous work on hybrid resonators has generally approximated the optical system as a single Lorentzian resonance.[37] In contrast, even the simplest hybrid resonators show Fano lineshapes in their response function,[38] responsible for the SERS enhancement factors. Thus, we expect SERS in hybrids to be controlled by a spectrally complex structure in LDOS, encompassing high-Q Fano lines and a low-Q plasmon-antenna-like contribution. Our semianalytical model correctly describes these intricate response functions over the entire frequency range, requiring only parameters from the bare resonators extracted from full-wave numerical modeling. Other approaches based on the Green tensor also allow us to derive Raman enhancements for complex photonic systems but rely on fully numerical calculations[6,11] or on a quasi-normal mode formalism.[10] Second, we extend this work from simple hybrid dielectric−photonic resonators to hybrids in which a single antenna hybridizes with multiple microcavity modes. This allows further control of SERS, through the accurate engineering of the structured photonic reservoir for Stokes, pump, and anti-Stokes frequencies independently. This scenario could be achieved with any whispering gallery mode (WGM) cavity system, with free spectral ranges that match vibrational frequencies.[39,40] Finally, a main generalization of our work over earlier works is that we include input−output channels. Indeed, in prospective molecular optomechanics experiments with hybrid dielectric photonic resonators, a waveguide can be specifically and efficiently interfaced with the cavity, to address hybrid resonances.[41] Using different input and output channels opens up new scenarios for detection schemes, like, for instance, pumping from free-space and collecting the Raman scattered power distributed over one or different output waveguide ports. This means that it is important to determine the ideal pumping and collection scheme. Our semianalytical model illustrates the potential and trade-offs for waveguide-addressable hybrid photonic−plasmonic resonators for physically relevant parameters for cavities and plasmon antennas taken from full-wave numerical modeling.[42] We derive realistic and quantitative predictions for SERS enhancements that can be compared with those obtained with the usual bare plasmon nanoparticle antennas. We finally show how the hybrid resonators will be a key platform to reach lower noise THz to visible transduction using molecular optomechanics and how the transduced signal is shared between the different output ports.

HYBRID MOLECULAR OPTOMECHANICS FORMALISM

We first consider a single-mode hybrid resonator composed of a plasmonic antenna coupled to a high-Q dielectric cavity (Figure 1). The model is based on semiclassical Langevin

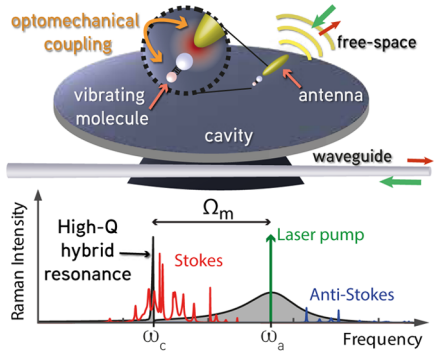

Figure 1. Raman scattering enhanced by a hybrid dielectric−plasmonic resonator. Top: sketch of a typical system: the spectrally narrow modes of a dielectric cavity hybridize with a plasmonic antenna resulting in high-Q small-mode-volume resonances, ideal for sideband resolved molecular optomechanics. Light can couple in and out through different ports such as the free-space or waveguides. Bottom: the hybrid system can be used to enhance both the laser pump and Raman sidebands, even in the sideband resolved regime, where the linewidth of the optical resonances are narrower than the mechanical frequency Ω_m.

equations[12,14] where a plasmonic antenna, described as a polarizable electrodynamic dipole scatterer, is coupled to a microcavity mode, quantified by a resonance frequency, mode volume, and intrinsic damping rate. In short, this model can be reduced to a description in terms of coupled equations of motion for two harmonic oscillators.[42] The single-cavity mode is described by the field amplitude $c(\omega)$ such that $|c(\omega)|^2$ is the normalized energy contained in the mode, with a resonance frequency ω_c and a damping rate κ. The excitation of the antenna is quantified by its induced dipole moment p, which derives from its polarizable nature. We assume a polarizability with resonance frequency ω_a, oscillator strength β, and a total damping rate $\gamma_a(\omega) = \gamma_i + \gamma_{rad}(\omega)$, taking into account intrinsic ohmic losses and frequency-dependent radiation losses assumed in vacuum $\gamma_{rad}(\omega) = \frac{\beta\omega^2}{6\pi\epsilon_0 c^3}$.[43] The dynamic antenna polarizability is then given by $\alpha_0(\omega) = \frac{\beta}{\omega_a^2 - \omega^2 - i\omega\gamma_a}$. Similarly to the cavity mode, the antenna field will be described by the field amplitude $a(\omega) = \frac{\omega}{\sqrt{2\beta}}p$. We consider each of the two optical resonators to be coupled to a unique port: a waveguide for the cavity mode and free space for the antenna. A vibrating molecule is placed in the hotspot of the antenna $\mathbf{r}_0$, and its vibration, corresponding to the stretching or compression of a specific molecular bond, is also described as a harmonic oscillator with a mechanical coordinate x_m, a resonance frequency Ω_m, and a decay rate Γ_m. The parametric Raman

https://doi.org/10.1021/acsphotonics.1c00808
ACS Photonics 2021, 8, 3506−3516

process is described as an optomechanical interaction between the molecule's vibration and the optical fields at its position.[12,14] The Langevin equations for the three harmonic oscillators (antenna, cavity, and mechanical modes) are written in the rotating frame of a laser pump of frequency ω_L (see the Supporting Information)

$$\begin{aligned}
&\dot{a} + (-\mathrm{i}(\omega_L - \omega_a) + \gamma_a/2)a - \mathrm{i}x_m(G_a a + G_{cross} c) - \mathrm{i}Jc = \sqrt{\eta_{in,a}\gamma_{rad}}\, s_{in,a}\\
&\dot{c} + (-\mathrm{i}(\omega_L - \omega_c) + \kappa/2)c - \mathrm{i}x_m(G_c c + G_{cross} a) - \mathrm{i}Ja = \sqrt{\eta_{in,c}\kappa}\, s_{in,c}\\
&\ddot{x}_m + \Omega_m^2 x_m + \Gamma_m \dot{x}_m - \frac{\hbar}{m}(G_a|a|^2 + G_c|c|^2 + G_{cross}(a^* c + a c^*)) = F_{ext}/m
\end{aligned} \tag{1}$$

In these equations, the cavity and antenna are linearly coupled through a hybridization strength $|J|$. This term describes the purely electromagnetic coupling between the two resonators: the antenna driving the cavity mode or the cavity polarizing the antenna. The magnitude of J depends on the confinement of the cavity field at the antenna position parametrized by the mode volume V_c, the oscillator strength of the antenna β, as well as the orientation of the antenna with respect to the cavity field polarization. It is written as $|J| = \frac{1}{2}\sqrt{\frac{\beta}{\epsilon_0 V_c}}$, where V_c is the effective cavity mode volume felt by the antenna $V_c = \frac{2}{\epsilon_0|\tilde{E}_c(\mathbf{r}_0)|^2}$, with $\tilde{E}_c(\mathbf{r}_0) = \mathbf{e}_p\cdot\tilde{\mathbf{E}}_c(\mathbf{r}_0)$ the normalized mode profile of the cavity field along the antenna polarization axis $\mathbf{e}_p$ at the position of the antenna, and simply written as $\tilde{E}_c$ in the following. The hybrid coupling then appears as a dipolar coupling rate between the antenna dipole and the cavity field.

The optomechanical coupling arises from a modification of the antenna and the cavity resonance frequencies due to the vibration of the molecule and is described by the optomechanical coupling strengths G_a and G_c between the molecule with either the antenna or cavity mode, and can be evaluated using first-order perturbation theory yielding[12]

$$G_{a,c} = \frac{\omega_{a,c}}{2\epsilon_0\epsilon V_{a,c}}\frac{\partial\alpha_m}{\partial x_m} = \frac{\omega_{a,c}}{4}|\tilde{E}_{a,c}(\mathbf{r}_0)|^2\frac{\partial\alpha_m}{\partial x_m} \tag{2}$$

where, similarly to the cavity mode, we have introduced an antenna effective mode volume $V_a = \frac{2}{\epsilon_0\epsilon|\tilde{E}_{a,c}(\mathbf{r}_0)|^2}$, with $\tilde{E}_a(\mathbf{r}_0)$ the normalized mode profile of the antenna, evaluated at the position of the molecule, and simply written $\tilde{E}_a$ in the following. The overlapping optical fields of the antenna and the cavity at the position of the vibrating molecule result in a crossed optomechanical coupling whose coupling strength can be approximated as $G_{cross} \simeq \sqrt{G_a G_c}$ (see the Supporting Information). Two different inputs are considered for the laser pump, either a free-space input where a far-field pump directly polarizes the antenna, or, waveguide input selectively exciting the cavity modes, with input amplitude and coupling efficiencies $s_{in,a}$ and $\eta_{a,in}$ for the antenna, and $s_{in,c}$ and $\eta_{in,c}$ for the cavity mode. The input amplitudes are normalized such that $|s_{in}|^2$ is the optical power entering at a given port. F_{ext} describes the input mechanical fields, which is here considered to be only thermal fluctuations. We thus arrive to the same coupled equations as derived by Roelli et al.,[12] however extended to take into account multiple optical modes and by adding the framework of input−output theory to the equations of motion, that can model different input and output channels. We note that while the equations and phenomena considered here are classical, they could readily be extended to include quantum fluctuations by introducing noise terms with appropriate correlators.

In the present work, we are only interested in the low-cooperativity regime, which is the most experimentally relevant,[12] and we can thus neglect the back-action of the optical fields on the mechanical resonance, i.e., consider only thermal−mechanical fluctuations x_m due to F_{ext}. The optical resonator amplitudes in the third equation of eq 1 will then be neglected, which discards the laser quantum back-action as well as dynamical back-action on the mechanical mode. The noise spectral density of the molecule's vibration is then given by the quantum Nyquist formula[44]

$$S_{xx}(\Omega) = x_{zpf}\Gamma_m\left[\frac{\bar{n}_{th}}{(\Omega - \Omega_m)^2 + (\Gamma_m/2)^2} + \frac{\bar{n}_{th} + 1}{(\Omega + \Omega_m)^2 + (\Gamma_m/2)^2}\right] \tag{3}$$

with the mean phonon occupation $n_{th} = \left(\exp\left(\frac{\hbar\Omega_m}{k_b T} - 1\right)^{-1}\right)$ for a bath at temperature T and the zero point amplitude x_{zpf}. These mechanical fluctuations will translate into optical Raman signal through the optomechanical coupling with the antenna and cavity modes as described by the two remaining Langevin equations for the optical fields. These can be linearized by decomposing the fields in a steady state plus a fluctuating part, $a \to \bar{\alpha}_a + a$, $c \to \bar{\alpha}_c + c$, and $x_m \to \bar{x}_m + x_m$. Finally, the small frequency shift due to the steady-state mechanical displacement $\bar{x}_m \sim 0$ is absorbed in the definition of ω_a and ω_c. The steady-state solutions were found by setting $a = c = 0$, and we get

$$\begin{cases}
\bar{\alpha}_a = \chi_a'\left(\sqrt{\eta_{in,a}\gamma_{rad}}\, s_{in,a} + \mathrm{i}J^*\chi_c\sqrt{\eta_{in,c}\kappa}\, s_{in,c}\right)\\
\bar{\alpha}_c = \chi_c'\left(\sqrt{\eta_{in,c}\kappa}\, s_{in,c} + \mathrm{i}J\chi_a\sqrt{\eta_{in,a}\gamma_{rad}}\, s_{in,a}\right)
\end{cases} \tag{4}$$

They correspond to the solution of a Rayleigh scattering process. The susceptibilities of the bare cavity mode χ_c and antenna mode χ_a are

$$\begin{cases}
\chi_a(\omega) = \frac{\mathrm{i}}{\omega - \omega_a + \mathrm{i}\frac{\gamma_a}{2}} = -\mathrm{i}\frac{2\omega}{\beta}\alpha_0(\omega)\\
\chi_c(\omega) = \frac{\mathrm{i}}{\omega - \omega_c + \mathrm{i}\frac{\kappa}{2}}
\end{cases} \tag{5}$$

The antenna and cavity response are modified by the hybrid coupling J, which yields new hybridized susceptibilities χ_c' and χ_a' for the two optical modes

$$\chi_{a,c}'(\omega) = \frac{\chi_{a,c}}{1 + |J|^2\chi_a\chi_c} \tag{6}$$

They can be seen as the bare constituents susceptibilities, dressed by an infinite series of antenna−cavity scattering events. The antenna having a very broad response compared to the cavity, the hybridized susceptibility χ_a', will display a Fano resonance at the frequency of the cavity.[45]

The fluctuating part of the field ($\Omega \neq 0$), responsible for the Raman scattering, is expressed in the frequency domain, and we keep only terms that are first order in the fluctuations (i.e., $x_m a$, $x_m c \to 0$)

https://doi.org/10.1021/acsphotonics.1c00808
ACS Photonics 2021, 8, 3506−3516

$$\begin{cases}\left(\omega_L + \Omega - \omega_a + i\frac{\gamma_a}{2}\right)a + Jc = -x_m(G_a\bar{\alpha}_a + G_{cross}\bar{\alpha}_c)\\ \left(\omega_L + \Omega - \omega_c + i\frac{\kappa}{2}\right)c + Ja = -x_m(G_c\bar{\alpha}_c + G_{cross}\bar{\alpha}_a)\end{cases} \tag{7}$$

Note that the fluctuations are evaluated at the frequency $\omega_L + \Omega$. To evaluate the Stokes or anti-Stokes sidebands, we will later set $\Omega = \mp\Omega_m$. The right-hand side of the equations shows that the source terms for the optical fluctuations arise from a sum of direct and crossed optomechanical coupling with the mechanical vibration. The first is given with a rate G_a or G_c, and the second through crossed optomechanical coupling G_{cross}; they are directly proportional to the steady-state solutions obtained previously. Both of these processes are described by an effective optomechanical coupling $G_{a,c}^{eff} = G_{a,c}\bar{\alpha}_{a,c} + G_{cross}\bar{\alpha}_{c,a}$ taking both the coupling rate and the steady-state solutions into account. We finally obtain the solutions for the fluctuations

$$\begin{cases}a(\omega_L + \Omega) = i\chi_a'(G_a^{eff} + iJ^*\chi_c G_c^{eff})x_m(\Omega)\\ c(\omega_L + \Omega) = i\chi_c'(G_c^{eff} + iJ^*\chi_a G_a^{eff})x_m(\Omega)\end{cases} \tag{8}$$

with all of the susceptibilities evaluated at the emission frequency $\omega_L + \Omega$. The antenna and cavity fluctuations a and c appear as a transduction of mechanical fluctuations x_m with a modified response due to the hybrid coupling characterized by J. The case with only a bare antenna corresponding to the usual SERS experiments is retrieved by setting $J = G_{cross} = 0$, yielding

$$a^{bare}(\omega_L + \Omega) = ix_m(\Omega)\chi_a(\omega_L)G_a\bar{\alpha}_a \tag{9}$$

Following the optomechanical formalism put forward in ref 12, with no back-action on the mechanical mode, we have arrived at a set of coupled classical equations where the optical fluctuations of the modes (inelastic process $\omega \neq \omega_L$) are driven by mechanical vibrations of the molecule.

Raman spectra scattered by the antenna to the far-field S_{ant} and the cavity to the waveguide S_{cav} can be immediately expressed as

$$\begin{cases}S_{ant}(\omega_D = \omega_L + \Omega) = \eta_{a,out}\gamma_{rad}|a(\omega_D)|^2\\ S_{cav}(\omega_D = \omega_L + \Omega) = \eta_{c,out}\kappa|c(\omega_D)|^2\end{cases} \tag{10}$$

where ω_D is the frequency of detection.

To obtain Raman enhancements factors, the spectra are normalized by the emission of the molecule in the homogeneous medium, in the absence of a resonator, given for the same excitation and collection conditions. This reference situation is modeled as the scattering of the Raman dipole of the molecule,[6] in which

$$p_R(\omega_D = \omega_L + \Omega) = \frac{\partial\alpha}{\partial x_m}x_m(\Omega)E_{inc}(\omega_L) \tag{11}$$

where E_{inc} is the incident field at the position of the molecule (see the Supporting Information). Using Larmor's formula,[46] one obtains the reference Raman scattered spectrum for the molecule in a homogeneous medium of index $n = 1$

$$S_{ref}(\omega_D, \omega_L) = \frac{\omega_D^4}{12\pi\epsilon_0 c^3}\left|\frac{\partial\alpha}{\partial x_m}\right|^2 S_{xx}(\Omega)|E_{inc}(\omega_L)|^2 \tag{12}$$

where we have replaced $|x_m|^2 \rightarrow S_{xx}$.

By replacing a and c by their expression of eq 8 and using eq 2, one can write the Raman spectrum of the antenna and the cavity as the product of three terms

$$S_{ant,cav} = \text{pump enh.} \times \text{LDOSC}_{ant,cav} \times S_{ref} \tag{13}$$

i.e., the reference spectrum S_{ref} enhanced both by a pump enhancement term and a collected LDOS (LDOSC) in either output port. The pump enhancement is given by

$$\text{pump enh.} = \left|\frac{\bar{\alpha}_a\tilde{E}_a + \bar{\alpha}_c\tilde{E}_c}{E_{inc}}\right|^2 \tag{14}$$

and corresponds to the field enhancement due to the optical hotspots compared to the incident field. The total field at the molecule's position (neglecting the incident field direct contribution) shows a coherent mixing of cavity and antenna contributions. The Raman emission is also enhanced by the collected LDOS, which, depending on the assumed collection channel, i.e., through the free-space or the waveguide port, reads

$$\begin{aligned}\text{LDOSC}_{ant}(\omega) &= \eta_{a,out}\gamma_{rad}\frac{3\pi\epsilon_0 c^3}{2\omega^2} \times \left|\chi_a'(\omega)(\tilde{E}_a^* + iJ^*\chi_c(\omega)\tilde{E}_c^*)\right|^2\\ \text{LDOSC}_{cav}(\omega) &= \eta_{c,out}\kappa\frac{3\pi\epsilon_0 c^3}{2\omega^2} \times \left|\chi_c'(\omega)(\tilde{E}_c^* + iJ^*\chi_a(\omega)\tilde{E}_a^*)\right|^2\end{aligned} \tag{15}$$

The total LDOS obtained by summing these two expressions can be cast as

$$\text{LDOS}_{tot} = \frac{3\pi\epsilon_0 c^3}{\omega^2}\,\text{Im}\sum_{j=a,c} i\chi_j'\left|\tilde{E}_j\right|^2 - 2J\chi_a'\chi_c\tilde{E}_a\tilde{E}_c^* \tag{16}$$

given by the sum of the LDOS of the hybridized antenna and cavity modes, along with a term arising from coherent interaction between the two resonators. The equality between the two equations is obtained only if $\eta_{out} = 1$, otherwise the intrinsic losses need to be added.

Both LDOSC expressions of eq 15 show a coherent coupling between antenna and cavity characterized by the effective susceptibilities

$$\chi_{a,c}^{eff} = (\tilde{E}_{a,c}^* + iJ^*\chi_{c,a}\tilde{E}_{c,a}^*)\chi_{a,c}' \tag{17}$$

that describe the hybrid response of each resonator in the presence of two coherently summed driving terms. They contain all of the spectral information governing the Raman spectra. Indeed, it can be shown that the pump enhancement of eq 14 can also be written as a function of the effective susceptibilities when pumping only through one port (free space or waveguide). The final Raman spectrum will then be a product of the effective susceptibility squared magnitudes evaluated at the pump and Raman-shifted frequencies

$$S_{ant,cav} \propto |\chi_{a,c}^{eff}(\omega_L)|^2|\chi_{a,c}^{eff}(\omega_D)|^2 \tag{18}$$

Using the molecular optomechanics formalism, we retrieve the second-order perturbation theory result relating the surface-enhanced Raman enhancement to the product of enhancement factor at the pump and emission frequencies.[4−6] A fine tuning

https://doi.org/10.1021/acsphotonics.1c00808
ACS Photonics 2021, 8, 3506−3516

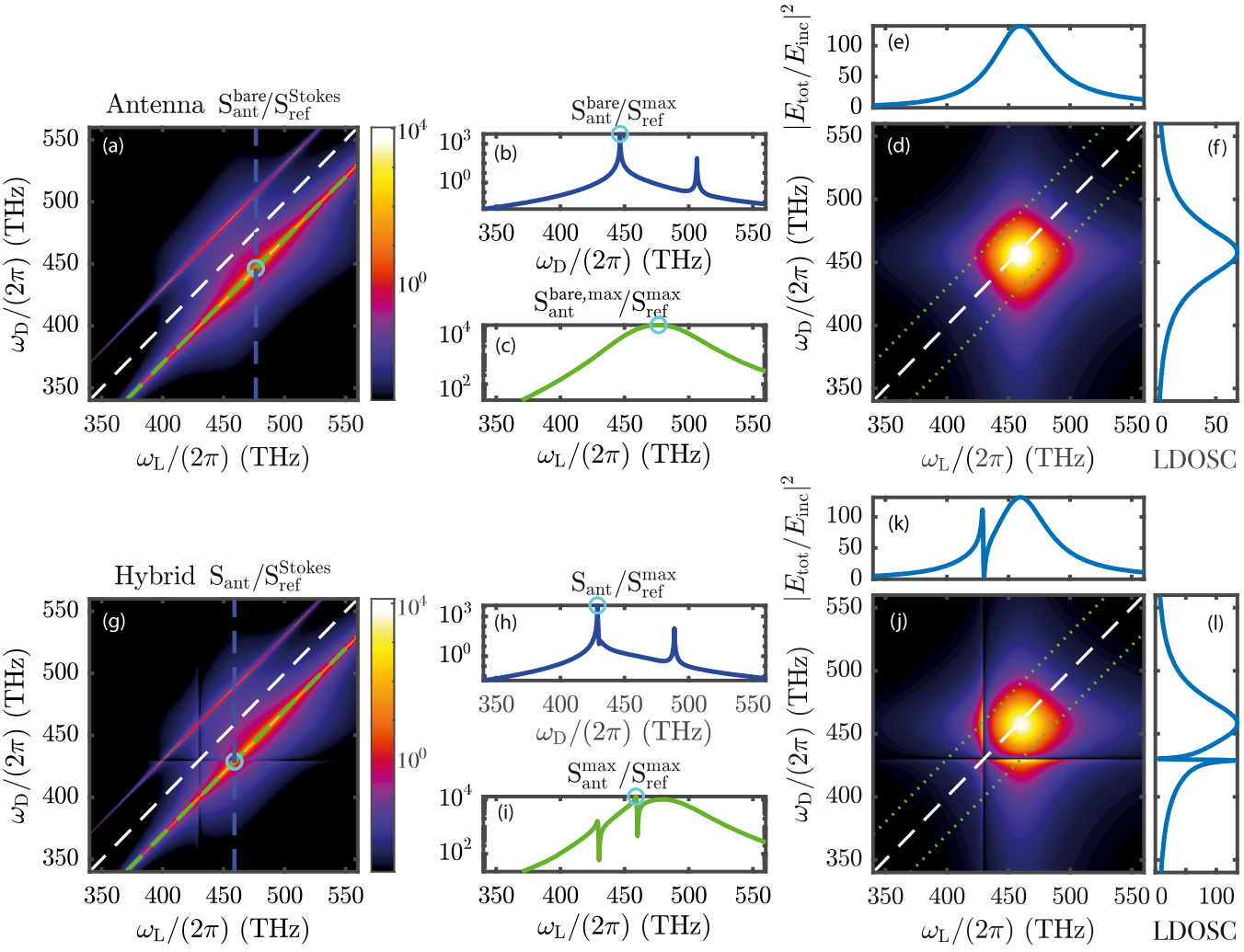

Figure 2. Raman spectrum enhanced by an antenna (a) as a function of the laser frequency, normalized by the Stokes emission peak of the molecules in air $S_{ref}^{Stokes}(\omega_L)$. The cross-cuts at the dashed blue and green lines correspond to (b) and (c). (b) Raman spectrum at the maximum enhancement and (c) antenna enhancement at the Stokes sideband as a function of the laser frequency. (d) Raman spectrum of the bare antenna S_{ant}^{bare}, normalized by the Raman emission of the molecules in air S_{ref} showing the antenna SERS enhancement as a function of the laser and detected frequencies. It is equal to the product of a pump enhancement term (e) and of a collected LDOS enhancement term (f). The case of a hybrid antenna−cavity resonator is given in (g)−(l), exhibiting narrow Fano resonances both in the Raman spectrum and in the pump and LDOS enhancements. See text for parameters.

of the antenna−cavity detuning is then essential to maximize the Raman enhancement of the hybrid. We have verified that the predictions of the model precisely match full-wave numerical simulation results, as shown in the Supporting Information.

RESULTS

Hybrid SERS Spectra. In Figure 2a, we plot the free-space Raman spectrum of an assumed Raman active species at a bare antenna $S_{ant}^{bare}(\omega_L, \omega_D)$, normalized by the Stokes peak amplitude of the same analyte in a vacuum environment as reference $S_{ref}^{Stokes} = S_{ref}(\omega_D = \omega_L - \Omega_m)$. The antenna parameters are $\omega_a/(2\pi) = 460$ THz, $\gamma_i/(2\pi) = 20$ THz, $\beta = 0.12$ C^2 kg^{-1} and an effective mode volume $V_a = 3\left(\frac{\lambda}{10}\right)^3$ corresponding to the values of a dipole placed at 10 nm away from a 50 nm radius gold sphere. Free-space input and collection are assumed to occur via a NA = 1 objective in vacuum, i.e., collection of the radiation in the upper half-space. This results in $\eta_{out} = 1/2$ and excitation $\eta_{in} = 1/10$ due to finite scattering cross section (see the Supporting Information). The molecular vibration frequency in this example is chosen as $\Omega_m/(2\pi) = 30$ THz, corresponding to typical Raman shifts of 1000 cm^{-1},[6] with quality factor $Q_m = 200$.

The antenna-enhanced Raman spectrum shows two sidebands appearing as diagonals at $\omega_D = \omega_L \mp \Omega_m$, i.e., the anti-Stokes and Stokes sidebands observed at the laser frequency shifted by the mechanical vibration resonance frequency. A vertical cut at the maximum intensity (blue dashed line) is shown in Figure 2b, representing a Raman spectrum at laser frequency fixed to the value at which the Stokes signal is most enhanced. The detected Stokes signal when scanning the laser frequency (green diagonal dashed line, detection frequency shifting in concert with the laser frequency) is shown in Figure 2c. As in usual SERS experiments,[6] the maximum enhancement is achieved when the pump frequency is set at $\omega_L = \omega_a + \frac{\Omega_m}{2}$, resulting in the best trade-off between pump enhancement taking place at $\omega_L = \omega_a$, and emission enhancement occurring at $\omega_D = \omega_a$. With the antenna and

https://doi.org/10.1021/acsphotonics.1c00808
ACS Photonics 2021, 8, 3506−3516

molecule position considered here, we obtain Raman enhancements on the order of 10^4, limited only by the effective mode volume of the antenna. We point out that this moderate Raman enhancement is only a consequence of the modest antenna parameters chosen in this work and that Raman enhancements up to 10^{10} are expected with state-of-the-art plasmonic antennas exhibiting nanometer-scale gap modes.[35,47] Indeed, for plasmonic antennas, and for the hybrids, the Raman enhancement will scale inversely as the mode volume of the antenna as it is shown in the Supporting Information. The effect of the photonic system is better visualized in Figure 2d, where we plot again the antenna-enhanced Raman spectrum S_{ant}^{bare}, but now normalized to the reference Raman spectrum $S_{ref}(\omega_D, \omega_L)$, to remove the dependence on the chosen mechanical vibration. We thus obtain the antenna enhancement compared to the homogeneous medium case for any pump and detection frequency. As it was derived for the hybrid case, the bare antenna Raman enhancement can be cast as a product of the pump enhancement $|E_{tot}/E_{inc}|^2$ and the collected LDOS, shown respectively in Figure 2e,f. Pump and LDOS enhancements for the bare antenna are obtained from eqs 14 and 15 by setting $J = G_{cross} = 0$. The pump enhancement depends on the laser frequency and the LDOSC on the detected frequency. High enhancements of the Raman process are obtained by enhancing both the pump at ω_L and the LDOS at $\omega_L + \Omega_m$, and are thus usually achieved with broad antenna resonances such that $\gamma_a > \Omega_m$, placing them by default on the sideband nonresolved system.

By a careful choice of parameters, the hybrid resonator allows to go beyond the limitation of sideband nonresolved optomechanics, yet obtain large SERS enhancement factors. The same figures of Raman scattering spectra in the case of a hybrid antenna-dielectric resonator are shown in Figure 2g–l, with a cavity red-detuned from the antenna by the mechanical vibration frequency $\omega_c/(2\pi) = (\omega_a - \Omega_m)/(2\pi) = 430$ THz corresponding to the Stokes sideband of the antenna, and a mode volume $V_c = 10\lambda^3$ and quality factor $Q_c = 10^3$. The main new feature is the appearance of a Fano resonance close to the cavity frequency, due to the interference of the coupled broad antenna resonance and the fine cavity resonance. This Fano feature is inherited both by the Raman spectrum, Figure 2h, and in the Stokes enhancement, Figure 2i, which show the capability of the hybrid system to obtain high enhancement with a high-Q resonance. Interestingly, the maximum Stokes enhancement is obtained for a laser tuned at $\omega_L = \omega_a$, the hybrid resonator allowing to enhance the pump with the antenna resonance, and the emission with the cavity resonance. Better insight follows from the Raman enhancement of the hybrid compared to homogeneous medium and shown in Figure 2j, which again is the product of a pump enhancement (Figure 2k) at the laser frequency and a collected LDOS enhancement (Figure 2l) at the detected frequency. Both quantities display a broad antenna-like resonance and a narrow Fano resonance arising from mixing with the cavity-like mode.

Choice of Optimum Read Out Scheme. In the rest of the article, we will focus on the Stokes (or anti-Stokes) enhancement curves, as the ones shown in Figure 2c,i, i.e., the detected frequency will be fixed at $\omega_D = \omega_L \mp \Omega_m$ as the laser frequency is scanned. In the case of the hybrid, the two different input and two different output ports result in four different Raman spectroscopy scenarios depending on whether the pump and collection are performed through the waveguide or in free space. The Stokes enhancement factors for the four different cases are presented in Figure 3, with the bare antenna response plotted in the dashed curve in panel a. The

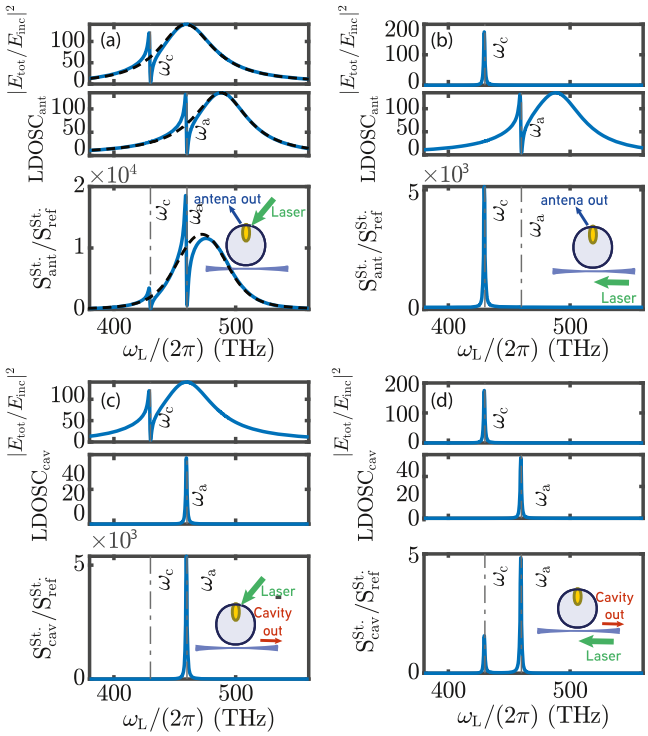

Figure 3. Stokes enhancement for the four different combinations of input−output as depicted on the sketches. Each Stokes enhancement (iii) is obtained as the product of the pump enhancement at ω_L (i) and the collected LDOS at $\omega_D = \omega_L - \Omega_m$ (ii) for the given input and output, respectively. The bare antenna response is plotted in the dashed curve in panel (a). The parameters are the same as in Figure 2.

parameters are the same as in Figure 2, with again a cavity red-detuned from the antenna by the molecule's vibration frequency, $\omega_c = \omega_a - \Omega_m$. The following observations can be made. First, the simultaneous excitation and read-out through the waveguide acts as a strong spectral filter at the cavity resonance. Since pump and Raman signal are at shifted frequencies, this filtering action intrinsically results in low overall SERS enhancements, 3 orders of magnitude below that offered by just an antenna in free space. Conversely, excitation and collection from free space result in a large SERS enhancement, roughly on the same scale as the SERS enhancement that the bare antenna provides, but still with improved numbers due to the simultaneous matching of pump and emission frequencies with one of the two resonators. However, the cavity mode elicits strong Fano features both when the pump and when the Stokes frequency go through cavity resonance. Finally, we consider the "mixed port" cases where either the pump goes via the waveguide and collection is via free space, or vice versa. Remarkably, the strongest pump field enhancement is reached when pumping through the waveguide and at cavity resonance $\omega_L \approx \omega_c$. For the chosen strongly blue-detuned cavity, the enhancement at the Stokes-shifted frequency for scattering in free space is modest due to the large detuning from antenna resonance, but nonetheless, the joint effect is a strong SERS peak. Conversely, detection through the waveguide requires tuning $\omega_L = \omega_c + \Omega_m$. The pump field is resonantly enhanced by the antenna, while the Raman signal collection into the waveguide is enhanced over a

https://doi.org/10.1021/acsphotonics.1c00808
ACS Photonics 2021, 8, 3506−3516

narrow band around $\omega_D = \omega_c$. The overall enhancement is similar to that in the reversed port choice to within a factor 2. This result can appear surprising since only one of the two configurations is doubly resonant and one would expect better enhancement factors in this case. However, the loss of enhancement due to a detuned antenna is compensated by the better output coupling efficiency for the antenna compared to the input coupling, $\eta_{in} = (1/5)\eta_{out}$ (see the Supporting Information). The waveguide allows better incoupling efficiencies than the antenna, but the collection efficiency can be, potentially, as good for the two.

To summarize, the hybrid system allows reaching Stokes enhancements of the same order of magnitude as the bare antenna case, but with much larger quality factors. Of particular interest for sideband resolved read out of vibrations is the case with collection through the waveguide where the Raman scattering is filtered by the narrow cavity resonance with enhancement factors similar to the case of free-space input and output. This allows us to explore the sideband resolved regime with high Raman enhancement.

Detuning Dependence. While coarsely speaking, the antenna and cavity frequencies need to be detuned by the mechanical vibration frequency $\omega_a - \omega_c = \pm\Omega_m$ to obtain the best enhancement factors, the fact that the enhancement is due to the product of Fano lineshapes imposes a finer analysis of the optimal detunings that are needed, and it is presented in the following. We focus here on the case where the cavity is red-detuned with respect to the antenna, and thus enhancing the Stokes sideband. Anti-stokes enhancement, requiring an inversed antenna−cavity detuning will be analyzed next.

Figure 4 presents the Stokes enhancement factor for the two different collection ports, when pumping through free space. The cavity−antenna detuning $\Delta_{ca} = \omega_c - \omega_a$ is changed by scanning the cavity frequency around $\omega_a - \Omega_m$, corresponding to the case considered in Figure 2. The cavity frequency is scanned by steps of 16κ, with, for each frequency, the Stokes enhancement shown as the product of the pump enhancement and LDOSC. Panels b and d show the maxima of the Stokes enhancement as a function of detuning, with each cross corresponding to the maximum Stokes enhancement of the same color in panels a and c, respectively. For both collection through free space or in the waveguide, the maximum achievable Stokes enhancement is obtained close to the intuitive detuning $\omega_c = \omega_a - \Omega_m$, but with some shift due to the Fano lineshapes. In the case of the waveguide output, an important contributor to the shift comes from an intrinsic asymmetry in antennas, namely, the fact that radiative losses into free space decrease at low frequencies, which facilitates a higher overall coupling into the waveguide. Concerning the tuning sensitivity, since one of the two resonances in play is still the broad antenna resonance, the needed precision in the antenna−cavity detuning remains on the order of the antenna linewidth.

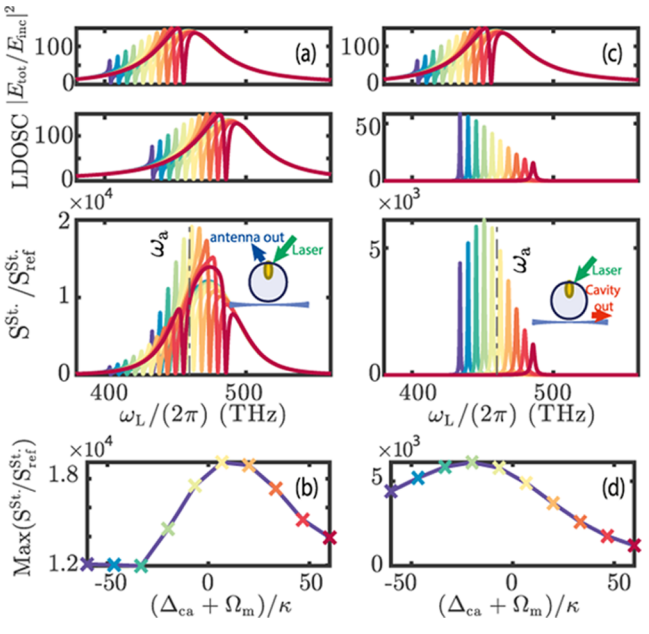

Figure 4. Influence of the cavity−antenna detuning Δ_{ca} on the Stokes enhancement for free-space input/output (a) and free-space input and waveguide output (c). The antenna frequency is fixed at $\omega_a/(2\pi)$ = 460 THz, and the cavity frequency is scanned around $\omega_a - \Omega_m$ in steps of 16κ. The maximum Stokes enhancement for each detuning is shown in (b) and (d) for the two collection cases, with the colored crosses corresponding to the respective colored plots in (a) and (c).

Choice of Cavity Parameters. An important question is how to choose the most appropriate cavity quality factor to reach the highest Raman enhancements. Aside from matching to the vibrational Q, the cavity Q will modify the in- and outcoupling ratio into the waveguide compared to free space. This is analyzed in Figure 5, where we plot the maximum pump enhancement and collected LDOS of eqs 14 and 15 as a function of the cavity quality factor Q_c. The antenna and cavity frequencies are $\omega_a/(2\pi)$ = 460 THz, and $\omega_c = \omega_a - \omega_m$, corresponding to the double resonant case for simultaneous pump and collection enhancement. Panels a and c first show the case of a fixed-mode volume $V_c = 10\lambda^3$ (as used throughout this work). It can be seen that for free-space input and output, the enhancement factors are increased for higher Q_c values

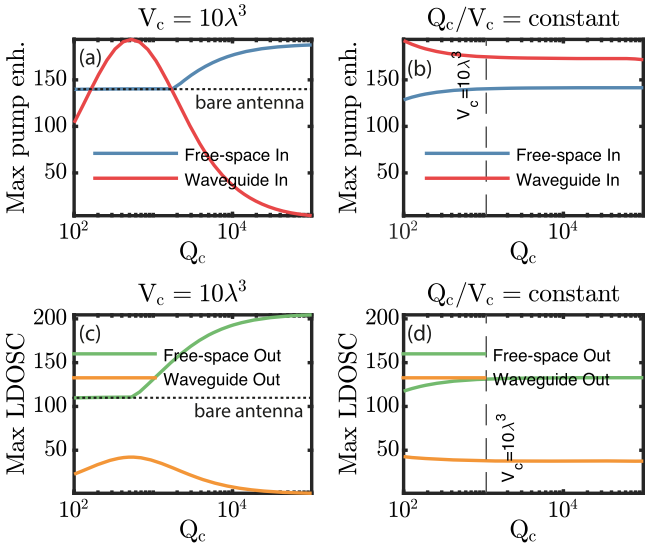

Figure 5. Maximum achievable pump enhancement (a, b) and LDOSC (c, d) as a function of the cavity quality factor Q_c for both input and output configurations; (a) and (c) are given for a fixed-mode volume $V_c = 10\lambda^3$, whereas (b) and (d) are given for a constant-cavity Purcell factor Q_c/V_c. The antenna frequency is $\omega_a/(2\pi)$ = 460 THz, and the cavity frequency is fixed at $\omega_c = \omega_a - \Omega_m$. The horizontal dotted line corresponds to the free-space case with only the bare antenna.

https://doi.org/10.1021/acsphotonics.1c00808
ACS Photonics 2021, 8, 3506−3516

since the Fano resonances sharpen to higher maximum values. Instead, for the case of waveguide input and output, there is an optimum at $Q_c \simeq 1000$ both for the pump enhancement and LDOSC. This is due to a trade-off with the cavity coupling efficiency that deterioriates for high Q_c while for too small Q_c, the LDOS enhancement will be small. The exact value of the best Q_c depends on the cavity mode volume V_c, which determines the hybrid coupling efficiency through $|J|^2 \propto 1/V_c$. For reference, we also show the case of constant Purcell factor Q_c/V_c cavity in Figure 5b,d. It is seen that the LDOS and pump enhancement are mostly constant for the whole range of Purcell factors, showing that the LDOS of the hybrid resonances only depend on the ratio Q_c/V_c.[42] This ratio is also proportional to $|J|^2/\kappa$, which appears in the denominator of eq 6 with $\chi_c(\omega_c) \propto Q_c$. This term dictates the hybrid interaction rate, and for constant Q_c/V_c, the interaction rate remains unchanged.

Anti-Stokes Detection. Enhancement of the anti-Stokes sideband can also be achieved with the hybrid resonator. To achieve the best collection in the waveguide, the cavity now needs to be blue-detuned with respect to the antenna mode. As shown in Figure 6, the enhancement is in this case slightly

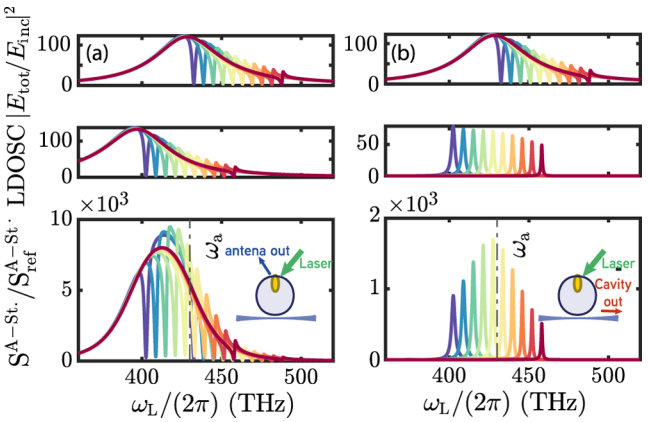

Figure 6. Anti-Stokes enhancement for different cavity−antenna detunings. The antenna is now red-detuned (ω_a = 400 THz) to enhance the pump, and the cavity frequency is scanned around the anti-Stokes sideband ($\omega_a + \Omega_m$) in steps of 16κ. The input is in free space, and the collection is either in free space (a) or in the waveguide (b).

smaller than for the Stokes enhancement case. This is due to the increased radiative losses γ_{rad} of the antenna at the (blue-shifted) collection frequency and a stronger emission from the reference dipole scaling as ω_D^4 as seen in eq 12. This has an impact for both collection paths, which still results in a comparable enhancement factor for the waveguide collection case compared to the free-space collection.

MULTIMODE CAVITIES

We have shown that the hybrid with a single dielectric mode is able to provide integrated collection of the Raman signal with good enhancement factors for both Stokes and anti-Stokes. Nevertheless, a fully integrated operation is prevented by the sideband resolution of the cavity that prevents from enhancing both the pump and the collection simultaneously through the waveguide. This issue can be resolved by working with multiple high-Q cavity modes, which allow both pump and collection enhancement. For instance, whispering gallery mode cavities provide multiple cavity modes addressable through the same waveguide. In this way, one could envision using two different cavity resonances to simultaneously enhance the pump and collection, by tuning the mode spacing to match the mechanical resonance frequency. The resulting Stokes enhancement factors are shown in Figure 7 for a hybrid with

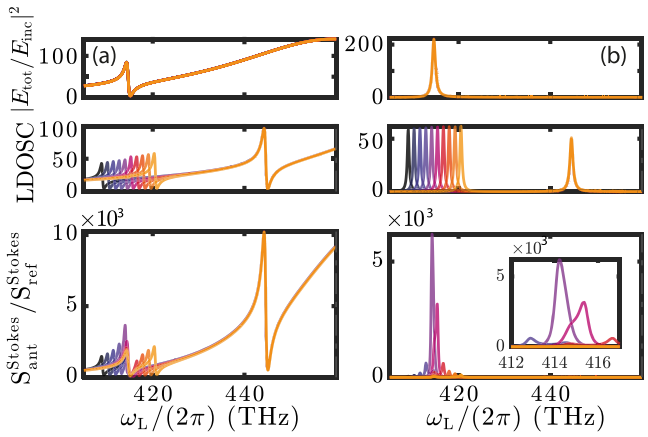

Figure 7. Stokes enhancement with a two-mode cavity and an antenna hybrid. The antenna is blue-detuned $\omega_a/(2\pi)$ = 460 THz with respect to both cavity modes. The first cavity mode serves as pump enhancement at $\omega_P/(2\pi)$ = 415 THz, and the Stokes sideband emission is enhanced by the second cavity mode, which is scanned around $\omega_P - \Omega_m$. We compare the cases with free-space-only (a) or waveguide-only (b) input and output. The Stokes enhancement is again the product of a pump enhancement factor and the collected LDOS. The inset in (b) shows a close-up of the best Raman enhancements close to $\omega_L = \omega_P$.

two cavity modes coupled to the same waveguide and an antenna coupled to free space. It can be shown that for multiple-resonant systems, the Raman enhancement can still be written as a product of the pump field enhancement by the hybrid and the collection LDOS in a given port, similarly to eq 13. We compare the cases of only free space addressing (a) with the fully integrated case (b). The first cavity mode is red-detuned, to enhance the collection, and is labeled C. The second cavity will serve to enhance the pump and is labeled P. Both cavity modes are then red-detuned compared to the antenna so as to work in the optimal regime where the radiative losses of the antenna are reduced. We have then from blue to red: $\omega_a/(2\pi)$ = 460 THz, $\omega_P/(2\pi)$ = 415 THz, and the frequency of the cavity mode use for collection scanned around the Stokes sideband of the former $\omega_C \simeq \omega_P - \Omega_m$ in steps of 1.1κ. We can see that the use of two cavity modes allows simultaneously a pump enhancement and an LDOS enhancement as shown in Figure 7b. This allows fully integrated Stokes enhancement factors that reach values equivalent to the Stokes enhancements of the bare antenna free-space configuration (in the order of 10^4 as seen in Figure 3a). This is furthermore obtained with high-Q resonances deep in the sideband resolved regime. Although the final enhancement—product of two hybridized cavity susceptibilities—necessitates fine frequency tuning on the order of κ, it allows for fully integrated Raman scattering with unspoiled enhancements.

OUTLOOK

The analogies with cavity optomechanics have resulted in exciting predictions of new phenomena in the field of SERS.

https://doi.org/10.1021/acsphotonics.1c00808
ACS Photonics 2021, 8, 3506−3516

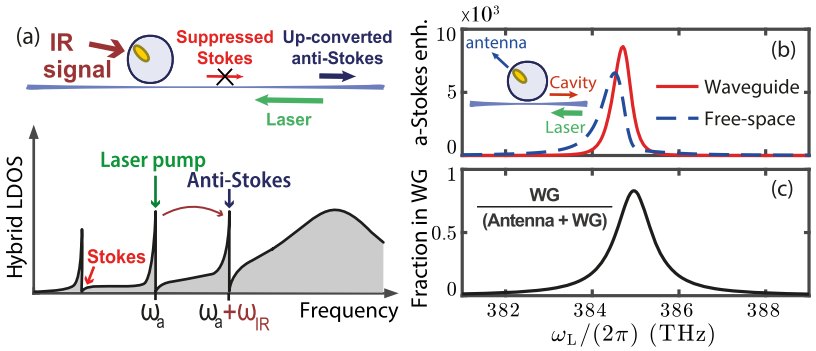

Figure 8. (a) Low-noise, integrated, IR-to-visible transduction using reservoir engineering. Using multiple cavity modes, one can selectively enhance the up-converted anti-Stokes while suppressing unwanted back-action noise. (b) Anti-Stokes enhancement with a two-mode cavity and an antenna hybrid. Parameters are the same as in Figure 7, with the laser now pumping the redder cavity. The red solid line corresponds to collection through the waveguide (fully integrated system), while the dashed blue line is for a collection through free space. (c) Integrated behavior: fraction of collected light into the waveguide (WG), reaching values up to 80% due to the Fano dip in the response function of the hybridized antenna.

Most of these new applications, such as dynamical back-action[12] and low-noise THz to optical transduction,[18] benefit from both a good optomechanical coupling, and sideband resolution, i.e., an optical linewidth smaller than the Raman shift. This implies having a resonator that has both small mode volumes and high-Q resonance. Hybrid dielectric and plasmonic resonances can achieve simultaneously these two requirements, exploiting both the small volume of a plasmonic antenna and the spectral confinement of dielectric cavities, with tunable parameters as a function of the detuning between the two resonators.[42]

We have developed a new formalism based on molecular optomechanics that allows us to calculate absolute Raman enhancement factor of a multimode hybrid system from simple parameters of the bare constituents. This represents in practice a substantial saving in computation time. Indeed, on the basis of a library of properties of N cavities, and M antennas, which will require $N + M$ simulations, we can predict the performance for all $N \times M$ combinations, and at any relative placement without further simulation. We intend this to be contrasted to full-wave-only approaches that will require each geometry to be simulated ($N \times M$ calculations, times the number of relative positions). The expressions obtained in this model explicitly show the interplay of pump and LDOS enhancement factors. We have then demonstrated that using experimentally available[36] hybrid systems, one can reach Raman enhancement factors equivalent to the bare plasmonic case, but in the sideband resolved regime, with optical linewidths orders of magnitudes smaller than the mechanical frequency. Additionally, our formalism correctly describes the coupling to different input and output ports, and we show that although optimal excitation and collection is reached through the antenna port, Raman enhancement for collection in the waveguide remains on the same order of magnitude. We have discussed the best choice of cavity parameters to optimize the Raman enhancement from the hybridized resonance. We showed that, for a given cavity mode volume, there is an optimal quality factor Q_c resulting from the trade-off of good incoupling and outcoupling rates and the strength of the cavity response function. More precisely, for realistic mode volumes of $V_c = 10\lambda^3$,[35] best integrated results are obtained for $Q_c \sim 1000$, easily accessible for any dielectric cavity.[36,48] Our model is readily applicable to experimental implementation using hybrid systems with dipolar plasmonic resonances. Best performances are predicted for antennas positioned near the cavity antinodes, increasing the hybrid coupling J, and for molecules as close as possible to the antenna hotspots, using, for example, self-assembled monolayers.[49] Finally, an efficient and fully integrated platform is proposed using simultaneously two different cavity modes, hybridized with a plasmonic antenna and coupled to same waveguide, each enhancing the pump and the collection respectively. Although we have here focused on the peak enhancement factors, the opportunities for Fano lineshapes are particularly exciting in quantum optomechanical applications employing reservoir engineering.[50] Recently, Roelli et al.[18] proposed molecular optomechanics for transduction of IR and THz radiation to visible light, with two very recent works showing experimental evidence for this.[22,23] By making use of Fano dips, it becomes possible to inhibit noise processes such as laser back-action-induced noise, i.e., vibrational pumping, greatly enhancing the signal-to-noise ratio for mechanical to visible transduction, as sketched in Figure 8a. This would allow us to push recent efforts in IR/THz to visible transduction[22,23] toward the quantum regime. With careful frequency tailoring, fully integrated quantum transduction could be obtained using multiple cavity modes, one inhibiting the Stokes and two enhancing the pump and the up-converted anti-Stokes photon. This will be the topic of future studies. In Figure 8b,c, we show an example of anti-Stokes enhancement, when pumping the system through the waveguide. The fraction of anti-Stokes photons emitted into the WG (fully integrated case) reaches values above 80%, with high Raman enhancement values above 10^3. Emission fractions into the WG above 95% can be easily obtained by increasing the Q_c/V_c ratio of the cavity by a factor 4 compared to our parameters, e.g., using a cavity with $Q_c = 4000$. In addition, we note that the similarities of our three-mode optomechanical model in this work with the model of photonic-molecule optomechanics[51,52] can lead to immediate applications, already demonstrated in more traditional optomechanical systems, such as phonon lasers[53−56] and unconventional single-photon devices.[57−60] Our semianalytical classical model is formulated such that it is easily translated into quantum mechanical equations of motion, solvable with, e.g., the Python toolbox QuTip.

■ ASSOCIATED CONTENT

Supporting Information

The Supporting Information is available free of charge at https://pubs.acs.org/doi/10.1021/acsphotonics.1c00808.

https://doi.org/10.1021/acsphotonics.1c00808
ACS Photonics 2021, 8, 3506−3516

Derivation of the Langevin equations, input−output parameters, influence of the antenna field confinement on SERS enhancement, and benchmark against full-wave simulations (PDF)

AUTHOR INFORMATION

Corresponding Author

A. Femius Koenderink − *Center for Nanophotonics, AMOLF, 1098 XG Amsterdam, The Netherlands;* orcid.org/0000-0003-1617-5748; Email: f.koenderink@amolf.nl

Authors

Ilan Shlesinger − *Center for Nanophotonics, AMOLF, 1098 XG Amsterdam, The Netherlands;* orcid.org/0000-0002-9328-1926

Kévin G. Cognée − *Center for Nanophotonics, AMOLF, 1098 XG Amsterdam, The Netherlands; LP2N, Institut d'Optique Graduate School, CNRS, Univ. Bordeaux, 33400 Talence, France*

Ewold Verhagen − *Center for Nanophotonics, AMOLF, 1098 XG Amsterdam, The Netherlands;* orcid.org/0000-0002-0276-8430

Complete contact information is available at: https://pubs.acs.org/10.1021/acsphotonics.1c00808

Author Contributions

[§]I.S. and K.G.C. contributed equally to this work.

Notes

The authors declare no competing financial interest.

ACKNOWLEDGMENTS

This work is part of the research program of the Netherlands Organisation for Scientific Research (NWO). The authors acknowledge support from the European Unions Horizon 2020 research and innovation program under Grant Agreements No. 829067 (FET Open THOR) and No. 732894 (FET Proactive HOT), and the European Research Council (ERC starting Grant No. 759644-TOPP). They also thank Javier del Pino and Philippe Lalanne for fruitful discussions and for their support.

REFERENCES

(1) Fleischmann, M.; Hendra, P.; McQuillan, A. Raman spectra of pyridine adsorbed at a silver electrode. *Chem. Phys. Lett.* **1974**, *26*, 163−166.

(2) Jeanmaire, D. L.; Van Duyne, R. P. Surface Raman spectroelectrochemistry: Part I. Heterocyclic, aromatic, and aliphatic amines adsorbed on the anodized silver electrode. *J. Electroanal. Chem. Interfacial Electrochem.* **1977**, *84*, 1−20.

(3) Albrecht, M. G.; Creighton, J. A. Anomalously Intense Raman Spectra of Pyridine at a Silver Electrode. *J. Am. Chem. Soc.* **1977**, *99*, 5215−5217.

(4) Wokaun, A. Surface-Enhanced Electromagnetic Processes. In *Solid State Physics*; Ehrenreich, H.; Turnbull, D.; Seitz, F., Eds.; Academic Press, 1984; Vol. *38*, pp 223−294.

(5) McFarland, A. D.; Young, M. A.; Dieringer, J. A.; Van Duyne, R. P. Wavelength-Scanned Surface-Enhanced Raman Excitation Spectroscopy. *J. Phys. Chem. B* **2005**, *109*, 11279−11285.

(6) Le Ru, E. C.; Etchegoin, P. G. In *Principles of Surface-Enhanced Raman Spectroscopy*; Le Ru, E. C.; Etchegoin, P. G., Eds.; Elsevier: Amsterdam, 2009; pp 185−264.

(7) Chu, Y.; Banaee, M. G.; Crozier, K. B. Double-Resonance Plasmon Substrates for Surface-Enhanced Raman Scattering with Enhancement at Excitation and Stokes Frequencies. *ACS Nano* **2010**, *4*, 2804−2810.

(8) Ye, J.; Wen, F.; Sobhani, H.; Lassiter, J. B.; Van Dorpe, P.; Nordlander, P.; Halas, N. J. Plasmonic Nanoclusters: Near Field Properties of the Fano Resonance Interrogated with SERS. *Nano Lett.* **2012**, *12*, 1660−1667.

(9) Yu, R.; Cox, J. D.; Saavedra, J. R.; Garciá De Abajo, F. J. Analytical Modeling of Graphene Plasmons. *ACS Photonics* **2017**, *4*, 3106−3114.

(10) Kamandar Dezfouli, M.; Hughes, S. Quantum Optics Model of Surface-Enhanced Raman Spectroscopy for Arbitrarily Shaped Plasmonic Resonators. *ACS Photonics* **2017**, *4*, 1045−1256.

(11) Zhang, Y.; Esteban, R.; Boto, R. A.; Urbieta, M.; Arrieta, X.; Shan, C.; Li, S.; Baumberg, J. J.; Aizpurua, J. Addressing molecular optomechanical effects in nanocavity-enhanced Raman scattering beyond the single plasmonic mode. *Nanoscale* **2021**, *13*, 1938−1954.

(12) Roelli, P.; Galland, C.; Piro, N.; Kippenberg, T. J. Molecular cavity optomechanics as a theory of plasmon-enhanced Raman scattering. *Nat. Nanotechnol.* **2016**, *11*, 164−169.

(13) Schmidt, M. K.; Esteban, R.; González-Tudela, A.; Giedke, G.; Aizpurua, J. Quantum Mechanical Description of Raman Scattering from Molecules in Plasmonic Cavities. *ACS Nano* **2016**, *10*, 6291−6298.

(14) Schmidt, M. K.; Esteban, R.; Benz, F.; Baumberg, J. J.; Aizpurua, J. Linking classical and molecular optomechanics descriptions of SERS. *Faraday Discuss.* **2017**, *205*, 31−65.

(15) Maher, R. C.; Galloway, C. M.; Le Ru, E. C.; Cohen, L. F.; Etchegoin, P. G. Vibrational pumping in surface enhanced Raman scattering (SERS). *Chem. Soc. Rev.* **2008**, *37*, 965−979.

(16) Zhang, Y.; Aizpurua, J.; Esteban, R. Optomechanical Collective Effects in Surface-Enhanced Raman Scattering from Many Molecules. *ACS Photonics* **2020**, *7*, 1676−1688.

(17) Benz, F.; Schmidt, M. K.; Dreismann, A.; Chikkaraddy, R.; Zhang, Y.; Demetriadou, A.; Carnegie, C.; Ohadi, H.; De Nijs, B.; Esteban, R.; Aizpurua, J.; Baumberg, J. J. Single-molecule optomechanics in "picocavities". *Science* **2016**, *354*, 726−729.

(18) Roelli, P.; Martin-Cano, D.; Kippenberg, T. J.; Galland, C. Molecular Platform for Frequency Upconversion at the Single-Photon Level. *Phys. Rev. X* **2020**, *10*, No. 031057.

(19) Palomaki, T. A.; Teufel, J. D.; Simmonds, R. W.; Lehnert, K. W. Entangling Mechanical Motion with Microwave Fields. *Science* **2013**, *342*, 710−713.

(20) Palomaki, T. A.; Harlow, J. W.; Teufel, J. D.; Simmonds, R. W.; Lehnert, K. W. Coherent state transfer between itinerant microwave fields and a mechanical oscillator. *Nature* **2013**, *495*, 210−214.

(21) Reed, A. P.; Mayer, K. H.; Teufel, J. D.; Burkhart, L. D.; Pfaff, W.; Reagor, M.; Sletten, L.; Ma, X.; Schoelkopf, R. J.; Knill, E.; Lehnert, K. W. Faithful conversion of propagating quantum information to mechanical motion. *Nat. Phys.* **2017**, *13*, 1163−1167.

(22) Chen, W.; Roelli, P.; Hu, H.; Verlekar, S.; Amirtharaj, S. P.; Barreda, A. I.; Kippenberg, T. J.; Kovylina, M.; Verhagen, E.; Martínez, A.; Galland, C. Continuous-Wave Frequency Upconversion with a Molecular Optomechanical Nanocavity. 2021, arXiv:2107.03033. arXiv.org e-Print archive. https://arxiv.org/abs/2107.03033.

(23) Xomalis, A.; Zheng, X.; Chikkaraddy, R.; Koczor-Benda, Z.; Miele, E.; Rosta, E.; Vandenbosch, G. A. E.; Martínez, A.; Baumberg, J. J. Detecting Mid-Infrared Light by Molecular Frequency Upconversion with Dual-Wavelength Hybrid Nanoantennas. 2021, arXiv:2107.02507. arXiv.org e-Print archive. https://arxiv.org/abs/2107.02507.

(24) Aspelmeyer, M.; Kippenberg, T. J.; Marquardt, F. Cavity optomechanics. *Rev. Mod. Phys.* **2014**, *86*, 1391−1452.

(25) Cohadon, P. F.; Heidmann, A.; Pinard, M. Cooling of a Mirror by Radiation Pressure. *Phys. Rev. Lett.* **1999**, *83*, 3174−3177.

(26) Giannini, V.; Fernández-Domínguez, A. I.; Heck, S. C.; Maier, S. A. Plasmonic Nanoantennas: Fundamentals and Their Use in Controlling the Radiative Properties of Nanoemitters. *Chem. Rev.* **2011**, *111*, 3888−3912.

(27) Ausman, L. K.; Schatz, G. C. Whispering-gallery mode resonators: Surface enhanced Raman scattering without plasmons. *J. Chem. Phys.* **2008**, *129*, No. 054704.
(28) Foreman, M. R.; Vollmer, F. Level repulsion in hybrid photonic-plasmonic microresonators for enhanced biodetection. *Phys. Rev. A* **2013**, *88*, No. 023831.
(29) Thakkar, N.; Rea, M. T.; Smith, K. C.; Heylman, K. D.; Quillin, S. C.; Knapper, K. A.; Horak, E. H.; Masiello, D. J.; Goldsmith, R. H. Sculpting Fano Resonances to Control Photonic-Plasmonic Hybridization. *Nano Lett.* **2017**, *17*, 6927−6934.
(30) Pan, F.; Smith, K. C.; Nguyen, H. L.; Knapper, K. A.; Masiello, D. J.; Goldsmith, R. H. Elucidating Energy Pathways through Simultaneous Measurement of Absorption and Transmission in a Coupled Plasmonic−Photonic Cavity. *Nano Lett.* **2020**, *20*, 50−58.
(31) Frimmer, M.; Koenderink, A. F. Superemitters in hybrid photonic systems: A simple lumping rule for the local density of optical states and its breakdown at the unitary limit. *Phys. Rev. B* **2012**, *86*, No. 235428.
(32) Kamandar Dezfouli, M.; Gordon, R.; Hughes, S. Modal theory of modified spontaneous emission of a quantum emitter in a hybrid plasmonic photonic-crystal cavity system. *Phys. Rev. A* **2017**, *95*, No. 013846.
(33) Barth, M.; Schietinger, S.; Fischer, S.; Becker, J.; Nüsse, N.; Aichele, T.; Löchel, B.; Sönnichsen, C.; Benson, O. Nanoassembled plasmonic-photonic hybrid cavity for tailored light-matter coupling. *Nano Lett.* **2010**, *10*, 891−895.
(34) Gurlek, B.; Sandoghdar, V.; Martín-Cano, D. Manipulation of Quenching in Nanoantenna-Emitter Systems Enabled by External Detuned Cavities: A Path to Enhance Strong-Coupling. *ACS Photonics* **2018**, *5*, 456−461.
(35) Palstra, I. M.; Doeleman, H. M.; Koenderink, A. F. Hybrid cavity-antenna systems for quantum optics outside the cryostat? *Nanophotonics* **2019**, *8*, 1513−1531.
(36) Doeleman, H. M.; Dieleman, C. D.; Mennes, C.; Ehrler, B.; Koenderink, A. F. Observation of Cooperative Purcell Enhancements in Antenna-Cavity Hybrids. *ACS Nano* **2020**, *14*, 12027−12036.
(37) Dezfouli, M. K.; Gordon, R.; Hughes, S. Molecular Optomechanics in the Anharmonic Cavity-QED Regime Using Hybrid Metal-Dielectric Cavity Modes. *ACS Photonics* **2019**, *6*, 1400−1408.
(38) Ameling, R.; Giessen, H. Microcavity plasmonics: strong coupling of photonic cavities and plasmons. *Laser Photonics Rev.* **2013**, *7*, 141−169.
(39) Soltani, S.; Diep, V. M.; Zeto, R.; Armani, A. M. Stimulated Anti-Stokes Raman Emission Generated by Gold Nanorod Coated Optical Resonators. *ACS Photonics* **2018**, *5*, 3550−3556.
(40) Liu, W.; Chen, Y.-L.; Tang, S.-J.; Vollmer, F.; Xiao, Y.-F. Nonlinear Sensing with Whispering-Gallery Mode Microcavities: From Label-Free Detection to Spectral Fingerprinting. *Nano Lett.* **2021**, *21*, 1566−1575.
(41) Peyskens, F.; Dhakal, A.; Van Dorpe, P.; Le Thomas, N.; Baets, R. Surface Enhanced Raman Spectroscopy Using a Single Mode Nanophotonic-Plasmonic Platform. *ACS Photonics* **2016**, *3*, 102−108.
(42) Doeleman, H. M.; Verhagen, E.; Koenderink, A. F. Antenna-Cavity Hybrids: Matching Polar Opposites for Purcell Enhancements at Any Linewidth. *ACS Photonics* **2016**, *3*, 1943−1951.
(43) Novotny, L.; Hecht, B. *Principles of Nano-Optics*; Cambridge University Press: Cambridge, 2006; pp 250−303.
(44) Barker, A. S.; Loudon, R. Response Functions in the Theory of Raman Scattering by Vibrational and Polariton Modes in Dielectric Crystals. *Rev. Mod. Phys.* **1972**, *44*, 18−47.
(45) Limonov, M. F.; Rybin, M. V.; Poddubny, A. N.; Kivshar, Y. S. Fano resonances in photonics. *Nat. Photonics* **2017**, *11*, 543−554.
(46) Jackson, J. D. *Classical Electrodynamics*, 3rd ed.; John Wiley & Sons: New York, 1999.
(47) Xomalis, A.; Chikkaraddy, R.; Oksenberg, E.; Shlesinger, I.; Huang, J.; Garnett, E. C.; Koenderink, A. F.; Baumberg, J. J. Controlling Optically Driven Atomic Migration Using Crystal-Facet Control in Plasmonic Nanocavities. *ACS Nano* **2020**, *14*, 10562−10568.
(48) Vahala, K. J. Optical Microcavities. *Nature* **2003**, *424*, 839−846.
(49) Bain, C. D.; Biebuyck, H. A.; Whitesides, G. M. Comparison of Self-Assembled Monolayers on Gold: Coadsorption of Thiols and Disulfides. *Langmuir* **1989**, *5*, 723−727.
(50) Yanay, Y.; Clerk, A. A. Reservoir engineering of bosonic lattices using chiral symmetry and localized dissipation. *Phys. Rev. A* **2018**, *98*, No. 043615.
(51) Kapfinger, S.; Reichert, T.; Lichtmannecker, S.; Müller, K.; Finley, J. J.; Wixforth, A.; Kaniber, M.; Krenner, H. J. Dynamic Acousto-Optic Control of a Strongly Coupled Photonic Molecule. *Nat. Commun.* **2015**, *6*, No. 8540.
(52) Schönleber, D. W.; Eisfeld, A.; El-Ganainy, R. Optomechanical Interactions in Non-Hermitian Photonic Molecules. *New J. Phys.* **2016**, *18*, No. 045014.
(53) Grudinin, I. S.; Lee, H.; Painter, O.; Vahala, K. J. Phonon Laser Action in a Tunable Two-Level System. *Phys. Rev. Lett.* **2010**, *104*, No. 083901.
(54) Jing, H.; Özdemir, S. K.; Lü, X.-Y.; Zhang, J.; Yang, L.; Nori, F. PT-Symmetric Phonon Laser. *Phys. Rev. Lett.* **2014**, *113*, No. 053604.
(55) Lü, H.; Özdemir, S. K.; Kuang, L.-M.; Nori, F.; Jing, H. Exceptional Points in Random-Defect Phonon Lasers. *Phys. Rev. Appl.* **2017**, *8*, No. 044020.
(56) Zhang, J.; Peng, B.; Özdemir, Ş. K.; Pichler, K.; Krimer, D. O.; Zhao, G.; Nori, F.; Liu, Y.-x.; Rotter, S.; Yang, L. A Phonon Laser Operating at an Exceptional Point. *Nat. Photonics* **2018**, *12*, 479−484.
(57) Liew, T. C. H.; Savona, V. Single Photons from Coupled Quantum Modes. *Phys. Rev. Lett.* **2010**, *104*, No. 183601.
(58) Snijders, H. J.; Frey, J. A.; Norman, J.; Flayac, H.; Savona, V.; Gossard, A. C.; Bowers, J. E.; van Exter, M. P.; Bouwmeester, D.; Löffler, W. Observation of the Unconventional Photon Blockade. *Phys. Rev. Lett.* **2018**, *121*, No. 043601.
(59) Vaneph, C.; Morvan, A.; Aiello, G.; Féchant, M.; Aprili, M.; Gabelli, J.; Estève, J. Observation of the Unconventional Photon Blockade in the Microwave Domain. *Phys. Rev. Lett.* **2018**, *121*, No. 043602.
(60) Li, B.; Huang, R.; Xu, X.; Miranowicz, A.; Jing, H. Nonreciprocal Unconventional Photon Blockade in a Spinning Optomechanical System. *Photonics Res.* **2019**, *7*, 630.

https://doi.org/10.1021/acsphotonics.1c00808
ACS Photonics 2021, 8, 3506−3516